www.czasopisma.pan.pl PAN POLSKA AKADEMIA NAUK www.journals.pan.pl

Arch. Min. Sci. **63** (2018), 4, 947-962

Electronic version (in color) of this paper is available: http://mining.archives.pl

DOI 10.24425/ams.2018.124986

JANUSZ WITALIS KOZUBAL*#, DEEPAK RAJ BHAT**,
PRACHAND MAN PRADHAN**

# LOAD BEARING CAPACITY OF LATERAL LOADED PILES IN WATERED CARPATHIAN FLYSCH

# PALE OBCIĄŻONE POZIOMO W NAWODNIONYM FLISZU KARPACKIM

In this paper, flysch is presented as a representative material of a wide section of the Carpathian Mountains, with some areas in Poland highlighted. The geological structure of this area is complex due to the alternating layers of blocky rock masses and soil (Vessia et al., 2017). Such a complex pattern is seen in some Alpine flysch slopes, such as the Ingelsberg landslide area (Romeo et al., 2015). Many authors are monitored, predicted landslides (Allasia et al., 2013; Bertacchini et al., 2009; Casagli et al., 2010) by sophisticated sensors. The rock-soil flysch successions have become intensively fissured as a result of their geological history, weathering (precipitation and snowmelt), and long-term water retention, especially on the surface layers. These complex materials are characterised by heterogeneous lithologies, whose mechanical properties are largely uncertain. These geological structures have also been confirmed by monitoring and control studies performed on a large number of landslides (Bednarczyk, 2014).

One of the most striking phenomena is the sudden decrease in the strength parameters in the studied rocks in the direction parallel to the layers due to watering. The process is made possible by heterogeneous fractured strong rock layers with high permeability coefficients for water. This study precisely describes the phenomena occurring at the contact area between the component layers of flysch under the wet conditions of a weak plane. An elastic-plastic analysis method that considers the developed strength model at the surfaces of the contact areas (Biernatowski & Pula, 1988; Pula, 1997) has been used to estimate the load capacity for piles working under a horizontal load. The piles are part of a reliability chain (Pula, 1997) in a given construction and are the first element of concern for monitoring (Muszynski & Rybak, 2017).

A particular device intended to study the dependence of the shear stress on a fixed failure surface in a controlled consolidation condition was utilized. The study was conducted for a wide range of displacements and for different values of stabilized vertical stresses of consolidation. The complexity of the processes occurring in the shear zone, presented as a detailed study of the material crack mechanics, is highlighted. The laboratory results were used to construct the mechanical model of the slip surface between the soil and rock with the description supported by a neural network (NN) approximation. The artificial NN was created as a multi-layered, easy to use approach for interpreting results and for quick reconstruction of approximated values useful for the calculations presented in laterally loaded piles. For the calculations, long, sheared strips of material were considered in a semi-analytical procedure to solve

* WROCLAW UNIVERSITY OF SCIENCE AND TECHNOLOGY WYB. STANISLAWA WYSPIANSKIEGO 27, 50-370 WROCLAW, POLAND

** DEPARTMENT OF CIVIL AND GEOMATICS ENGINEERING, KATHMANDU UNIVERSITY, DHULIKHEL 45200, NEPAL

# Corresponding author: Janusz.Kozubal@pwr.edu.pl

a differential equation of stability. The calculations are intended to reveal the safety indexes for a wide range of boundary tasks as the most significant indicator for design decisions.

**Keywords:** Piles, soil tests, limit load, Layered rock, Carpathian flysch

Flisz karpacki jest formacją występującą na znacznym obszarze Europy Środkowej, stwarza znaczne zagrożenie podczas nawodnienia np. przez infiltrację wody deszczowej lub awarię drenażu. Dla opisu zniszczenia tego materiału o regularnej strukturze z naprzemiennie ułożonych warstw słabych i mocnych, przedstawiono model. Jest to dogodna do zastosowania koncepcja, zaprezentowana w zadaniu stateczności poziomo obciążonych pali. Model można stosować dla szerokiego zakresu skłonu warstw jak i sposobu powiązania głowic pali z oczepem. Ważnym elementem pracy jest opis powierzchni poślizgu między warstwami z zastosowaniem wyników badań laboratoryjnych na próbkach gruntów zarówno sztucznie wytworzonych, jak i pobranych z osuwisk. Badania przeprowadzono w zmodyfikowanym obrotowym aparacie bezpośredniego ścinania. Przykłady obliczeniowe ilustrują procedury modelowania dla słabych skał wraz z ich interpretacją.

**Słowa kluczowe:** pale, flisz karpacki, badania gruntu, stateczność

# Flysch in the European Carpathian range

## Geological formation characteristics

Carpathian Flysch was originally formed from the process of turbidity deposition of rock. The soil mixture was transported from the shore zone of a shallow warm sea or from the inland via streams. The sedimentation clastic process occurs along the stream trajectory. The soil material was separated into fractions as a function of their distance from the origin point (finer grains remained on the bottom after a longer distance than that travelled by larger grains). Periodic changes in the supply conditions (i.e., along the shore zone and time) caused alternate settling of layers and consequently different gradations and thicknesses of soils, which resulted in layers. The process of lithification formed sandstones from the sand layers, gravels through cementation created conglomerates, and clays metamorphosed into shale (Dzulynski et al., 1959). The Polish flysch deposits are divided into the following major groups (Collins et al., 2011):

- normal flysch, consisting of adjacent sandstone and shale beds of approximately equal thicknesses;
- shale flysch, where shale beds are thicker than the adjacent sandstone beds; and
- sandstone flysch, where sandstone beds are thicker than the adjacent shale beds.

The portion of the Carpathian range located in the southern region of Poland is the focus of the article. This area is part of the Carpathian thrust and fold range that belongs to the territory of Austria in the west, Poland in the north, and Serbia in the southeast (Fig. 1). Its laminar structure provokes landslides, with an example of its scale being Sawicki, which is located on the southern slope of the Maślana Hill in Szymbark (Rączkowski, 2004). The Maślana Góra hill is formed by the flysch of the Magura Nappe and is composed of glauconitic sandstones, Ciężkowice sandstones, shales (variegated, red and green), marls, and conglomerates. The Sawicki landslide covers a 1.62 km$^2$ area and is 2850 m in length and 385 m in height, with a total volume

of displacement material of 25 million m3, as described by Kiszka (2016) and Chowaniec et al. (1977). The beginning of this landslide dates back to the end of the XVIII century.

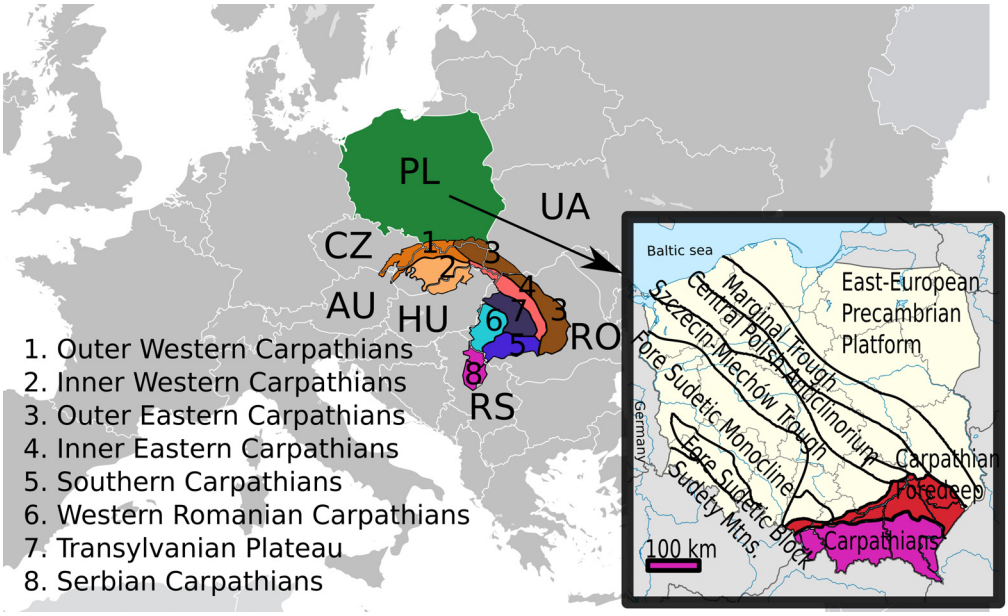


Fig. 1. Carpathian Mountains. In the lower right corner,
the principal Poland tectonic units are shown, and the Carpathian regions are marked

Four morpho-dynamic zones can be detected in the Carpathian Flysch slopes with different surface deposits (Broniatowska & Gaszyński, 2006; Margielewski et al., 2010): high mountains, middle mountains, foreland and sub-mountain zones. Structural models of Carpathian Flysch are assumed as sequences.

According to Broniatowska and Gaszyński (2006), the Carpathian Flysch formations can be grouped into five structural models, as shown in Fig. 2. These models include prevalent hard rock blocks greater than 0.3 m thick (Fig. 2(**1.a**)) or less than 0.3 m thick (Fig. 2(**1.b**)), sandstones and clay shale alternations (Fig. 2(**2.a**), Fig. 2(**2.b**), Fig. 2(**3.a**) and Fig. 2 (**3.b**)), and a loose structure with sandstone layers consisting of a few sandstone blocks (Fig. 2(**4**), Fig. 2(**5**)).

The stratigraphic settings of the rocky slope in Carpathian Flysch involved in failure mechanisms observed by Broniatowska and Gaszyński (2006) are shown in Figs. 3 (**a**)-(**f**): strong rocky layers are joined by a weaker lamina layer made of softer flysch. Thus, the slope can be modelled as a sequence of thin flysch soils and thick sandstone layers; soil strata are considered to be boundary surfaces among the rocky blocks (Fig. 3).

The variable and irregular structural settings shown in Fig. 2 and Fig. 3 are addressed hereafter by applying a reliability analysis. All the illustrated models with the exception of number 5 in Fig. 2 can be represented by a sequence of rocky and soil layers with variable thicknesses and mechanical properties. The case of sandstone bricks, which implies a three-dimensional structural model, is not investigated due to its irregular pattern.

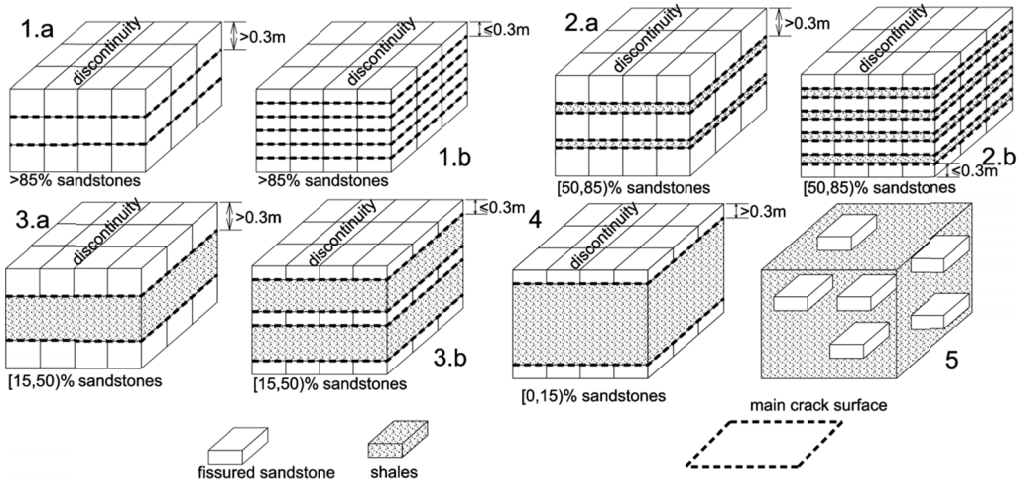


Fig. 2. Structural models of Carpathian Flysch from Broniatowska and Gaszyński (2006): (**1.a**) 85-100% sandstones and thick layers of hard rock >0.3 m thick. (**1.b**) 85-100% sandstones and thin layers of hard rock <0.3 m thick. (**2.a**) 50-85% sandstones and thick layers of hard rock >0.3 m thick. (**2.b**) 50-85% sandstones and thin layers of hard rock >0.3 m thick. (**3.a**) 15-50% sandstones and thick layers of hard rock >0.3 m thick. (**3.b**) 15-50% sandstones and thin layers of hard rock >0.3 m thick. (**4**) Less than 15% sandstones with thick layers. (**5**) Less than 15% sandstones with loose structures

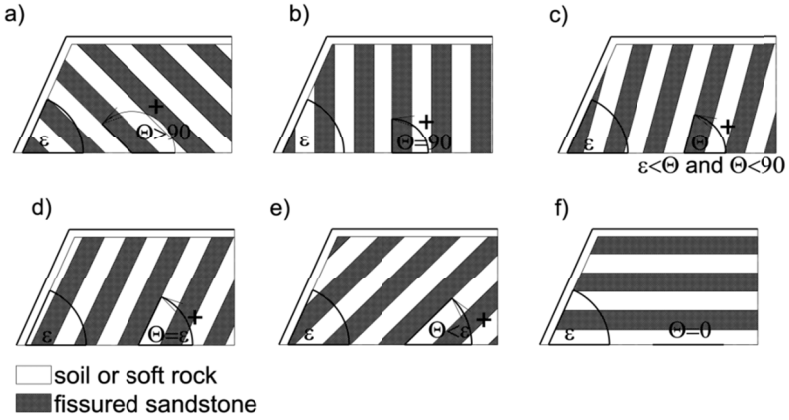


Fig. 3. Schematic of possible geological settings in the flysch Carpathian Mountain involved in actual instability failure ($\varepsilon$ = slope inclination, $\Theta$ = layer inclination): (**a**) asequent, (**b**) vertical, (**c**) (**d**) insequent, (**e**) consequent, and (**f**) horizontal layers.

## Slip surface between sandstone and clayey shale

The term shale is defined as wide range of originally clayey material, which after consolidation, transverse to sedimentary rocks. Shale is composed of compacted clay or silty clay that commonly breaks along bedding planes, and is often no thicker than paper rinds. Shales are the

most abundant type of all sedimentary rocks, and as presented in the description of Carpathian Flysch, they are a problematic component of this complex rock from a geoengineering point of view. Clay minerals account for approximately 50-60% (Shaw & Weaver, 1965; Hillier, 2006) of the total weight, and they are often responsible for many of the problems encountered when drilling through shales. Clayey shales in contact with a water bed were simulated using pure clayey compacted soil in a laboratory experiment. This approach is also a good approximation for other types of shales, such as the finest-grained detrital soft rocks based on plastic clays framework, which occur in young rock formations. The assumption of the determined watered contact surface is the main reason for using a special laboratory parametric research.

## Description of the test samples

In this study, four typical clayey soil samples were taken (Bhat et al., 2013; 2014). One sample of kaolin clay was commercially available, and the other three clayey soils were collected from large-scale landslide sites. The first soil sample was confirmed to have a comparatively high amount of smectite and was designated as "Clayey Soil-I." . The second sample was confirmed to have a comparatively high amount of chlorite and was designated as "Clayey Soil-II." Similarly, the third sample was confirmed to have a comparatively high amount of mica and was designated as "Clayey Soil-III." Similarly, the kaolin clayey was designated as "Clayey Soil-IV." The plasticity index of Clayey Soil-IV was the highest, followed by Clayey Soil-I, Clayey Soil-II, and then Clayey Soil-III. The physical properties of the typical clayey soils are presented in Table 1.

TABLE 1

Physical properties of the tested samples

| Sample name | Solid density, $G_s$ (g/cm$^3$) | Liquid limit , LL (%) | Plastic limit, PL (%) | Plasticity index, PI (%) | Soil classification (%) | | |
|---|---|---|---|---|---|---|---|
| | | | | | <2 µm | 2 µm-75 µm | 75 µm-425 µm |
| **Clayey Soil-I** | 2.65 | 96.5 | 59.0 | 37.5 | 24 | 18.0 | 58.0 |
| **Clayey Soil-II** | 2.75 | 47.5 | 31.2 | 16.3 | 20 | 68.1 | 11.9 |
| **Clayey Soil-III** | 2.74 | 34.1 | 20.7 | 13.4 | 21 | 59.7 | 19.3 |
| **Clayey Soil-IV** | 2.72 | 52 | 22 | 30 | 74 | 26 | 0 |

The overall flow of the experiment is shown in Fig. 4. The data from the results were collected by an electronic recording management system in a pure numeric form for interpretation.

The results of the laboratory tests are shown in Fig. 5 for all soils samples in terms of shear stress versus shear displacement. Initially, a sharply increasing value of the shear stress reaches a maximum value (the peak). With a constantly increasing linear displacement, a decrease in shear stress was observed, followed by a stabilization of the residual values. The final residual values are from 21.9% for Soil I to 88.1% for Soil IV in comparison to the peak. For other cohesive soils, this phenomenon has also been confirmed experimentally. The described contacts are used for further calculations with assumed average stresses in the material comparable to the experimental value, equal to 98.1 kN/m$^2$. Further experimental work will extend the applicability the model to a wider range of normal stress and velocity of shearing.

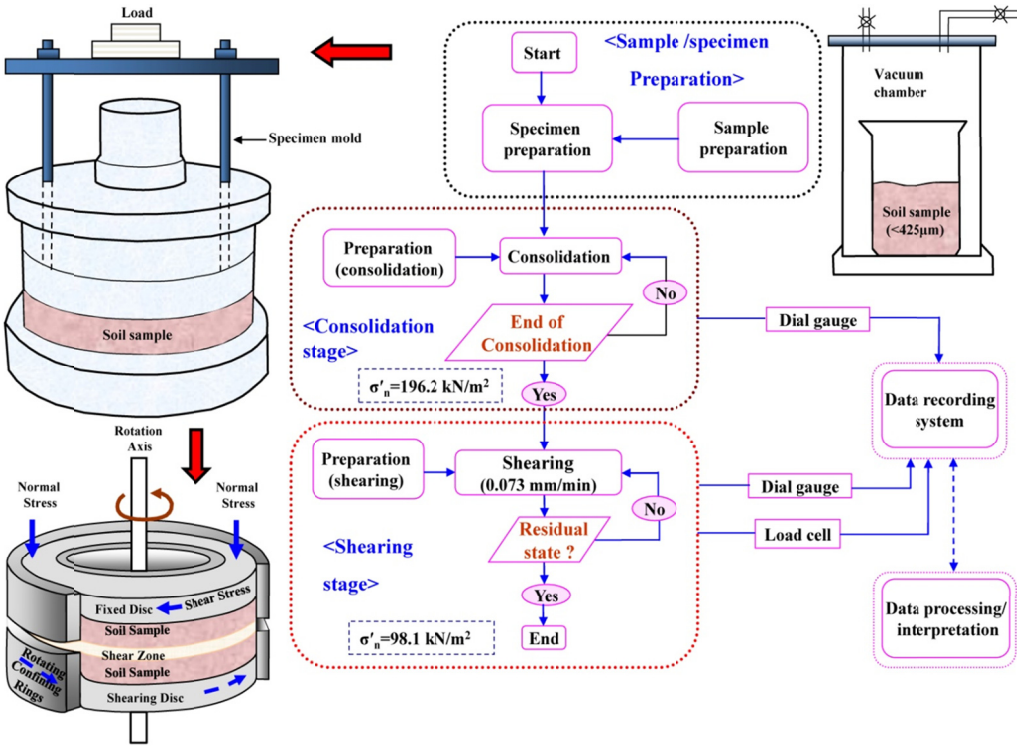


Fig. 4. Overall experimental flow of the shearing rate test

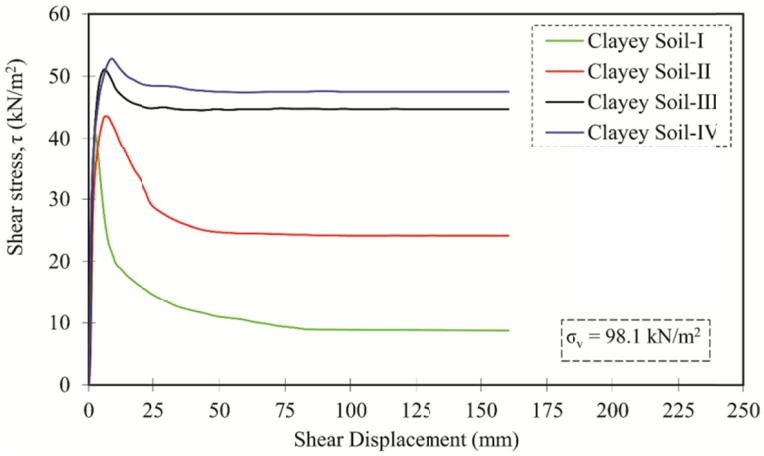


Fig. 5. Typical results of the shearing rate test of the tested samples

## Mechanical behaviour approximation of clayey soils

Accordingly, the approximated material function is described by the cross section of the Mohr-Coulomb strength criterion by the following non-linear regression model for a constant vertical pressure value $\sigma$:

$$\tau_0(\gamma,\sigma) = \tau_0(\varepsilon,\sigma,\mathbf{b}) + err \tag{1}$$

where $\varepsilon$ is an independent variable of shear deformation, $\mathbf{b}$ is a vector of $k$ unknown parameters of the regression model, $\tau_0(\varepsilon,\sigma,\mathbf{b})$ is the function, and $err$ is a random variable describing the estimation error. The normal stress $\sigma$ has a constant value. The components of vector $\mathbf{b}$ are determined by minimising the sum of the squared differences between the given and predicted values as follows:

$$\mathrm{Var}(\tau_0) = \sum_{i=1}^{n} (\tau_{0i} - \tau_0(\varepsilon,\sigma,\mathbf{b}))^2 \tag{2}$$

where $\gamma$ represents the vector of the input data, $\tau_0(\varepsilon,\sigma,\mathbf{b})$ are the approximated values according to Eq. (1), and $\tau_{0i}$ are the known measured values at $\varepsilon_i$ in the laboratory tests measured for different soils under a normal stress equal 98.1 kN/m$^2$, with $n$ being the total number of automatically digital registered points.

A NN method was used to derive the material model approximation. This method is well recognised in engineering applications and is resistant to errors.

Hereafter, an NN with hyperbolic tangent activation functions was used. A three-layered NN with one hidden layer containing 2-5 neurons was required in order to obtain satisfactory results. This type of NN is able to approximate the functions of independent variables characterised by a wide range of variation. Accordingly, five input variables in the first layer were assumed to be independent random variables. The following approximation is obtained from the NN:

$$\tau_0(\varepsilon,\sigma,\mathbf{b}) \approx \sum_{j=0}^{K} b_{1+3j} \tanh(b_{2+3j}\varepsilon + b_{3+3j}) + b_{4+3j} \tag{3}$$

where $K$ is the number of neurons in the hidden layer, $\mathbf{b}$ is the vector of weights, which are trained in the learning process, and $\varepsilon$ is a vector of variables and $\tau_0$ is a shear forces approximation. The composed method was used to determine the unknown vector $\mathbf{b}$ for 4 neurons (16 elements). The starting values of $\mathbf{b}$ were randomly assigned in a loop procedure to minimize the LMA error, as it was not classical in the NN training back propagation error procedure.

The approximation for the Soil I sample:

$$\begin{aligned}\tau_0(\sigma,\varepsilon,\mathbf{b}) \approx {} & -37.86 \tanh(1.347 - 1022\,\varepsilon) + \\ & + 44.53 \tanh(0.120 - 236.9\,\varepsilon) - 16.78 \tanh(0.166 + 23.84\,\varepsilon) + \\ & + 32.15 \tanh(315.6 + 4279\,\varepsilon)\end{aligned} \tag{4}$$

where $\gamma$ is the displacement, and $\mathbf{b}$ is the vector of fitted parameters.

For Soil II:

$$\begin{aligned}\tau_0(\sigma,\varepsilon,\mathbf{b}) \approx {} & -4.265 \tanh(1242 - 283837\,\varepsilon) - 21.29 \tanh(1.295 - 1182\,\varepsilon) + \\ & + 12.97 \tanh(0.968 - 66.9\,\varepsilon) + 11.688 \tanh(28.03 + 2767\,\varepsilon)\end{aligned} \tag{5}$$

For Soil III:

$$\tau_0(\sigma,\varepsilon,\mathbf{b}) \approx -32.90 \tanh(0.658 - 791\ \varepsilon) + 2.465 \tanh(3.249 - 261.7\ \varepsilon) + \\ + 55.6 \tanh(183.9 + 1740\ \varepsilon) - 41.276 \tanh(26.03 + 5525\ \varepsilon) \quad (6)$$

For Soil IV:

$$\tau_0(\sigma,\varepsilon,\mathbf{b}) \approx 1.334 \tanh(4.671 - 329\ \varepsilon) - 196 \tanh(2.864 + 9.208\ \varepsilon) + \\ + 445.7 \tanh(1.442 + 493.9\ \varepsilon) - 201.3 \tanh(581.6 + 35198\ \varepsilon) \quad (7)$$

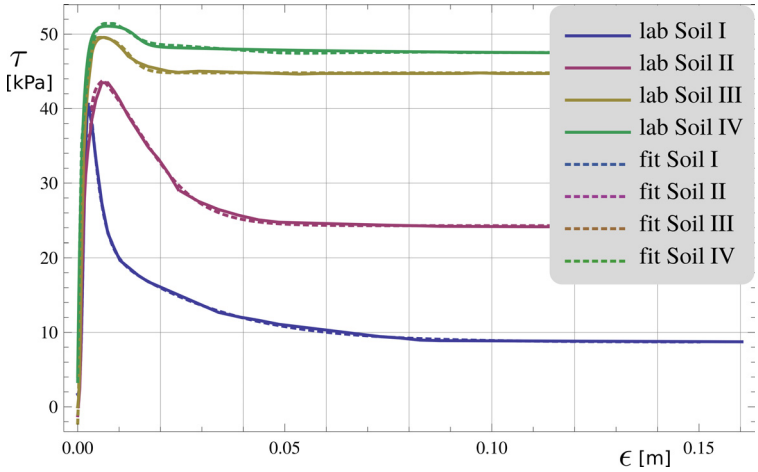


Fig. 6. Fitting results for Eq. (4) to (7) as dashed lines in comparison to laboratory lines (see also Fig. 5)

Almost perfect fittings are presented in Fig. 6. The analytical functions demonstrated in Eq. (4) to (7) are convenient for solving an equilibrium differential equation.

## Pile stability in the Carpathian Flysch

### Equilibrium state for sliding slices

In this study, calculations are conducted for the model depicted in Fig. 7 corresponding to structural models of the Carpathian Flysch from Fig. 2. The presented method is adequate for modelling (excluding the case of Fig. 2(**5**)) full range compositions of sandstone boulders into shale mass. The geological settings from Fig. 3 in the Carpathian Mountain Flysch can be used with the assumed mechanism and method considered here. The initiation of the destruction process has two origins separately analysed as a type of relocation of the socketed material into the layered material pile via a rotational or parallel move. Both variants are sketched in Fig. 7, where (**a**) is the rotational type, typical for a jointed connection between pile heads and a slab; and (**b**) it is a pure slip only along the contact lines (joints) adequate for fixed connections between a slab and pile heads. That instability cases are investigated according to an elastic-plastic approach.

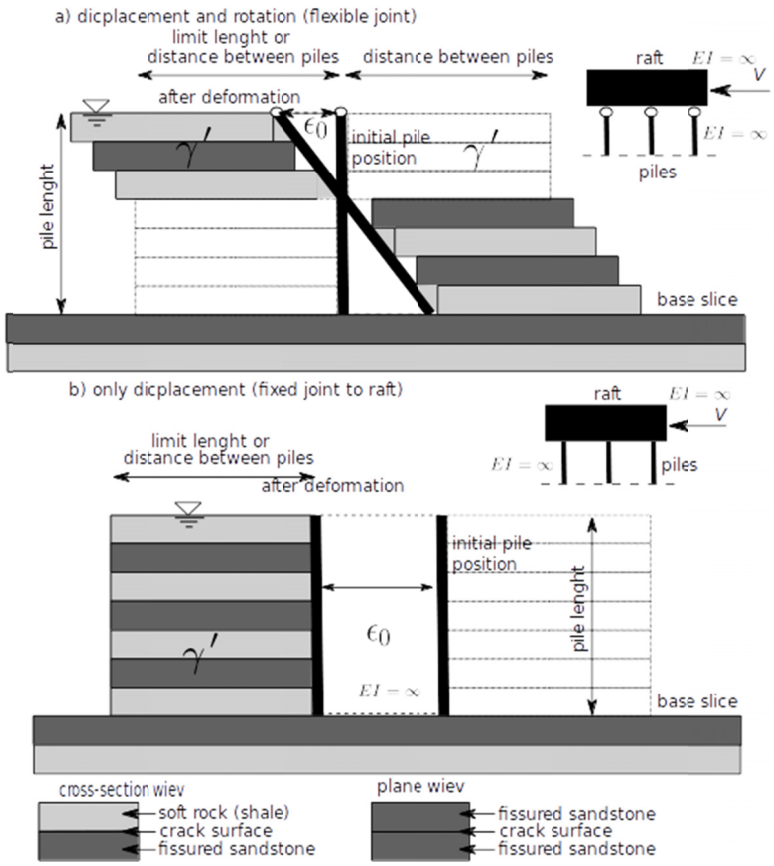


Fig. 7. Sketch of the structural model considered in this case study for parallel layers sliding by contact with pile heads: (**a**) joined to slab , (**b**) fixed to slab

The assumptions for building a mechanical model of the Carpathian Flysch were as follows:

1. Fissured sandstone represents an ideal elastic model; it is fissured and the connection among the sandstone particles is treated as frictional.
2. Clayey shale is defined as an ideal elastic-plastic material with plasticity work based on the volume change omitted in the calculation as the weak layer; it fills the space between the sandstone strati.
3. Contact between the weak and strong layers of flysch is described by an approximated plastic law described in previous sections and measured externally in laboratory experiments.

Rock slices under the deformation process are sheared along the surface, as presented in Fig. 8. In the case of sliding cracks into sandstone in Fig. 8(**b**), $D$ is a dimension between the closest outside parallel cracks to the pile cross-section shape ($D_p$ is the diameter of the pile). For the next calculation it was assumed that $D = D_p$. The largest variant of parallel cracks into sandstone was intentionally analysed (Hoek & Brown, 1980; Barton, 1986) with the assumptions

that destructed surfaces exist (in regular fissured rock) and that joints are persistent, as described in Kim et al. (2007). The mechanical dependencies between the shear stress and strain are based on the residual shear value as a maximum, $R_{res}$, and it is intended to simulate the intrinsic mechanism of damage for the watered rock-joints under the assumption that the influence of gravity to the normal pressure in the vertical joint-cracks is equal to zero. As per Jaeger et al. (2007) the condition for slippage on the considered plane of weakness is:

$$\tau_1 = R_{res} + \mu_w \sigma_n \tag{8}$$

where $\mu_w = \tan\phi$. The values of the shear strength of filled discontinuities and filling materials were according to Barton (1974). Loosened sandstone blocks during the compression process behave like a perfectly elastic material where $E_r$ is the Young's modulus. Between the edge of the moving rock and soil (shale), the fixed contact breaks, becoming a place for dissipate plastic work.

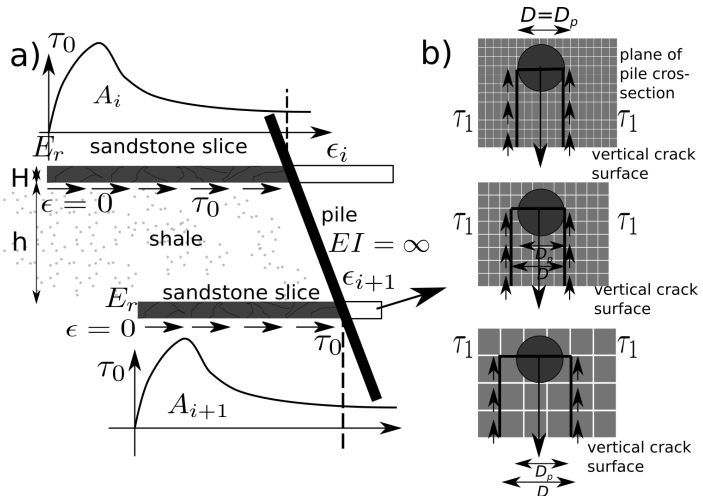


Fig. 8. Destruction mechanism between the shifting slices of the layered material, basic dimensions and marking (**a**) mechanical description of the continuous material model with contact lines, (**b**) band involved in the shearing process (plane view)

After periods of intense rainfall, the strength parameters of the flysch rock are reduced. The appearance of water in the fissured sandstone means that the water in the heterogeneous fissured rock penetrated into the contact zones, which are deep in the vertical profile. The shear stresses on the surface are approximately described by Eq. (4) to (7). After considering the forces of gravity, an ordinary differential equation is obtained as:

$$d\varepsilon = -dl\left(\tau_0(\varepsilon\cos\Theta, b)D + 2H\tau_1 - \gamma(H+h)D\sin\Theta\right)\frac{1}{HE_rD} \tag{9}$$

where $d\varepsilon$ is the change of infinitesimal length $dl$ in the compressed zone, $D$ is defined as the Fig. 8(**b**) dimension, $H$ is the thickness of the sandstone layer, $h$ is the thickness of the shale layer, $\gamma$ is the average specific gravity for flysch in a mass, and $\Theta$ is the inclination of layers (Fig. 3).

The solution of the differential equation is determined numerically, due to the form of the function approximating the mechanical model of the material. The distance at which the frictional forces are in equilibrium to the external force that causes deformation $\varepsilon_0$ is obtained from the formula:

$$L_{\lim} = \int_0^{\varepsilon_0} \frac{HE_r D d\varepsilon}{\left(\tau_0(\varepsilon \cos\Theta, b)D + 2H\tau_1 - \gamma(H+h)D\sin\Theta\right)} \tag{10}$$

This distance determines the scope of the impact of the foundation pile on the slope and nearby trenches, and it is measured parallel to the inclination of layers Θ. The force that is necessary for displacement of the strip is quantified using Hook's law along the distance $0 - L_{\lim}$. Fig. 9 shows the results of a single strand of laminar substrate consisting of two layers of rock equivalent to the one contact surface. In this example the parameters were set as $H = 0.10$ m, $E_r = 150$ MPa, $\tau_1 = 50$ kPa, $D = D_p = 0.40$ m, $h = 0.5$ m, and $\gamma = 24.0$. The three components cooperate together: $\tau_0$ plus $\tau_1$ minus the force of gravity. The calculations were made for bands with a distribution of the friction bar according to a non-linear regression for all discussed soil samples (I-IV). Fig. 9 presents the maximum length $L_{\lim}$ [m] for different inclinations without any mechanical or geometrical limits. Fig. 10 shows the summary of forces corresponding to deformations for laminar layers of different inclinations.

Calculations were also made for the scheme proposed in Fig. 7 for piles cooperating with each other under a horizontal load. This scheme limits the maximum length of the slip surfaces.

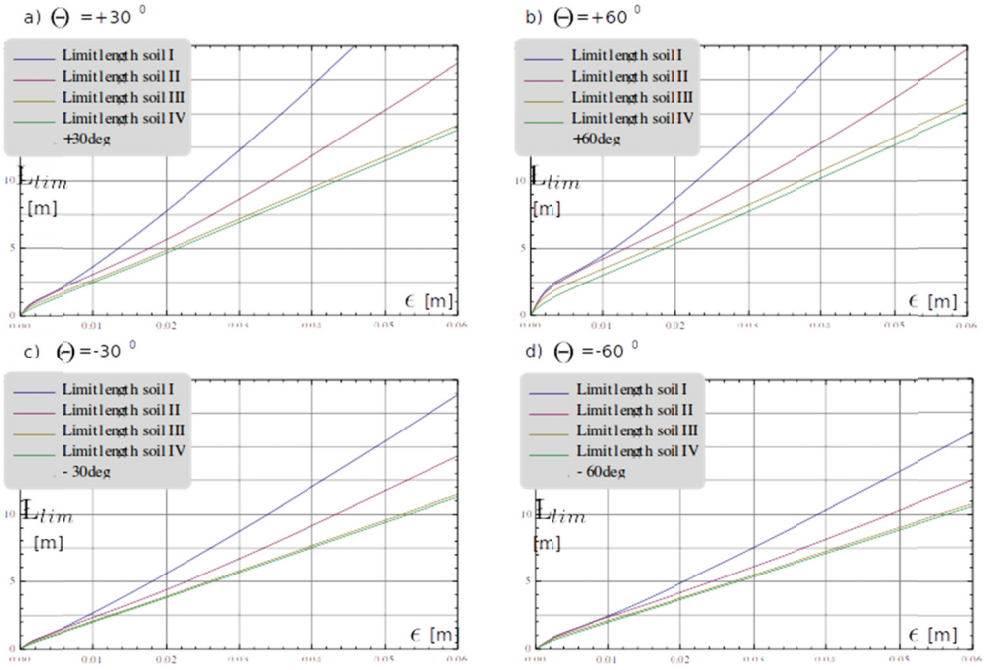


Fig. 9. The values of length $L_{\lim}$ of slices when the initiation of the $\varepsilon_0$ displacement process of shear is equilibrated: (**a**) Θ = +30°, (**b**) Θ = +60°, (**c**) Θ = –30° and (**d**) Θ = –60°

To estimate the impact of this limitation on the value of the forces generated at the contact surface to be determined numerically, the solution of Eq. (8) that includes $\varepsilon_0$ and $\varepsilon_k$ is applied as follows:

$$\varepsilon_k \rightarrow \int_{\varepsilon_k}^{\varepsilon_0} \frac{HE_r Dd\varepsilon}{\left(\tau_0(\varepsilon\cos\Theta, b)D + 2H\tau_1 - \gamma(H+h)D\sin\Theta\right)} - L_k = 0 \tag{11}$$

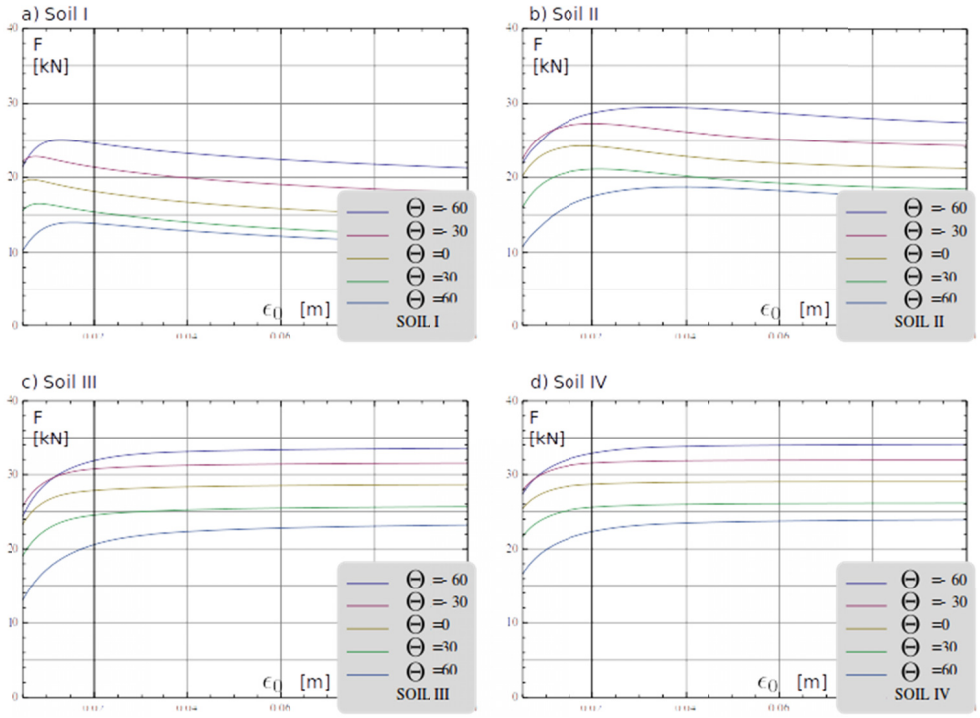


Fig. 10. The value of forces F [kN] in strips with a length $L_{\text{lim}}$ as a function of the displacement $\varepsilon_0$ for the various inclination of layers $\Theta = \{-60°, -30°, 0°, 60°, 30°\}$ for: (**a**) soil I, (**b**) soil II, (**c**) soil III, (**d**) soil IV

On the limited distance $L$, we again use Hook's law to calculate the maximum possible force $F_0$ generated on a sandstone slice. The results are presented as percentages in Fig. 11, where $F$ is the force generated on $L_{\text{lim}}$. As in previous cases, the calculation results are provided for all soils.

## Solution for horizontal loaded pile cap in the flysch bed

Three significant example calculations were evaluated for the described pile cap model on a watered flysch. Previously discussed variants of pile head connections to a slab were analysed as shown Fig. 12. In the first case, Fig. 12(**a**), the initial displacement is $\varepsilon_0$, along an ideal rough pile was a determining unity inclination displacement between the layers of flysch. The joint works as a perfect rotary. All layers worked under similar mechanical conditions, with the same value of a generated force $E_0$ in $H$ (sandstone layer and $h$) and in the shale layer (Eq. (11)). For

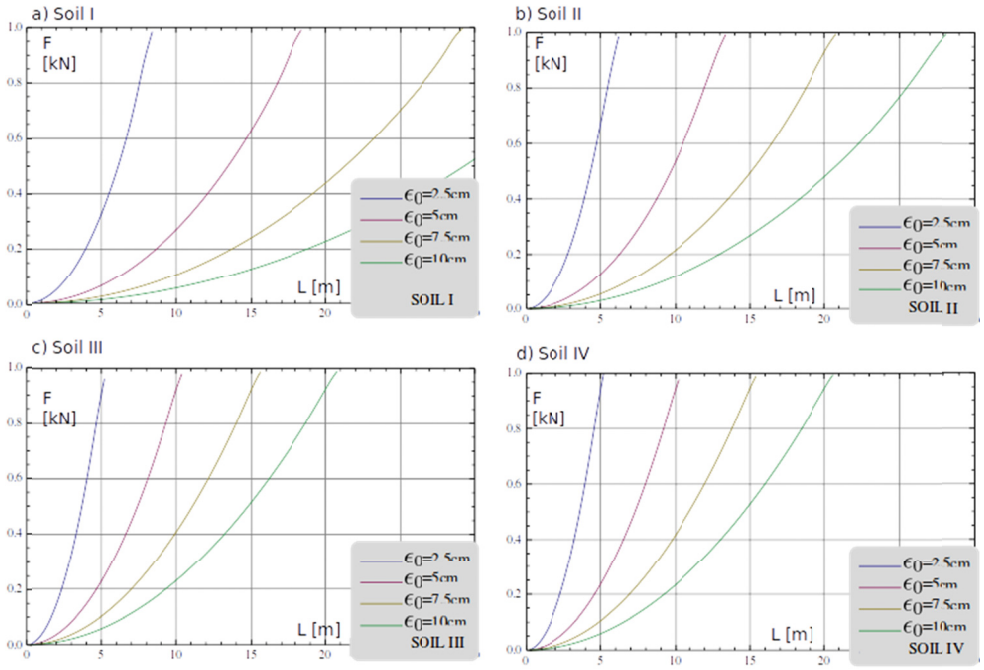


Fig. 11. Reduction forces $F_0/F$ on length L: (**a**) soil I, (**b**) soil II, (**c**) soil III, (**d**) soil IV ($F_0$ – force for L length, $F$ – force for $L_{\text{lim}}$ length)

the value of $\varepsilon_0$ and the corresponding $L_k$ from Eq. (8), the maximum horizontal force $E_{\max}$ can be calculated assuming that the pile is much longer than the thickness of the lamina layers, and the value of the passive pressure can be obtained as:

$$e_0 = \frac{E_0}{H + h} \tag{11}$$

For the equilibrium of a bending moment, the result of the pile length $L_p$ assumes a constant vertical pressure value for all contact layers that is equal to 98.1 kPa (adequate for the assumed value of the laboratory contact tests) and that is generated in the base slice force $R_j$:

$$\alpha = \sqrt{\frac{L_p^2}{2} + \frac{R_j L_p}{e_0}} \tag{12}$$

The second condition for horizontal forces of the static balance is:

$$F_j = e_0(2a - L_p) - R_j \tag{13}$$

The case from Fig. 12(**b**) gives the reaction collected along the pile length and an equal force generated into base slices:

$$M_f = R_f \frac{L_p}{2},\ F_f = R_f \tag{14}$$

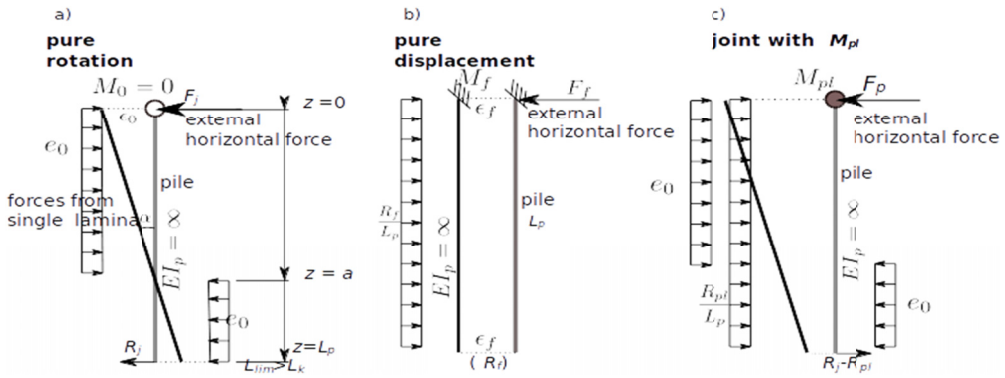


Fig. 12. Equilibrium for a joint with (**a**) full pivot possibility; (**b**) infinity stiffness; and (**c**) pivot limited by a plastic bending moment

The last most common and useful configuration is in Fig. 12(**c**) where the connection to a pile cap may be loaded by a maximum plastic bending moment $M_{pl}$. This form was assumed as an algebraic sum of forces in both cases in Fig. 12(**a**) and Fig. 12(**b**). For the calculations, a mixed mechanism was adapted with $M_{pl} = R_j L_p$ and with a safe assumption of a concentrate reaction in the foot of a pile. For a pile with a length of 5.0 m, the results are presented in Fig. 13 in a graphical form. The maximum values of $\varepsilon_0$ are quite large, but they were selected due to the quick decrease in structure stiffness, which indicates system instability.

In the second analysed mechanical case of pile heads fixed by a slab as shown in Fig. 12(**b**), the entire process is on a single surface slip at the level of the pile feet, and the torque is transferred by an infinitely rigid connection to the pile head. As in the previous task, a zero value for the layer inclination was used.

## Conclusions

The developed and presented deterministic semi-analytical method for calculating the load bearing capacity is the first step in exploring a wide set of limiting tasks important for mining industry. The examples were rock slope stability, rock cutting, anchor locking, and dam stability under climate influences. This analysis was performed for pile-supported construction, especially in response to the many noticed failures connected to the deterioration of the Carpathian Flysch in the Lower Beskids. This method can also be applied in a wide range of rigid mounted-type piles, from fixed to perfect rotary joints of piles with a slab. The method is based on laboratory test results for weak rocks with a calibrated apparatus to measure slip forces. The elastic-plastic model of the rock material with a limit load method helps to quickly determine the values of the forces and displacement limits for pile caps in soft fractured rocks. This approach is an alternative to the numerical method with the advantages of low time consumption and a possibility for direct use in a reliability calculation. The method concentrates on the mechanical parameters, which decrease significantly at the contact surfaces due to hydration and result in a privileged slip surface direction that was incorporated into the presented solution. The method incorporates several classes of structural discontinuities of a massive rock. The approach was constructed as

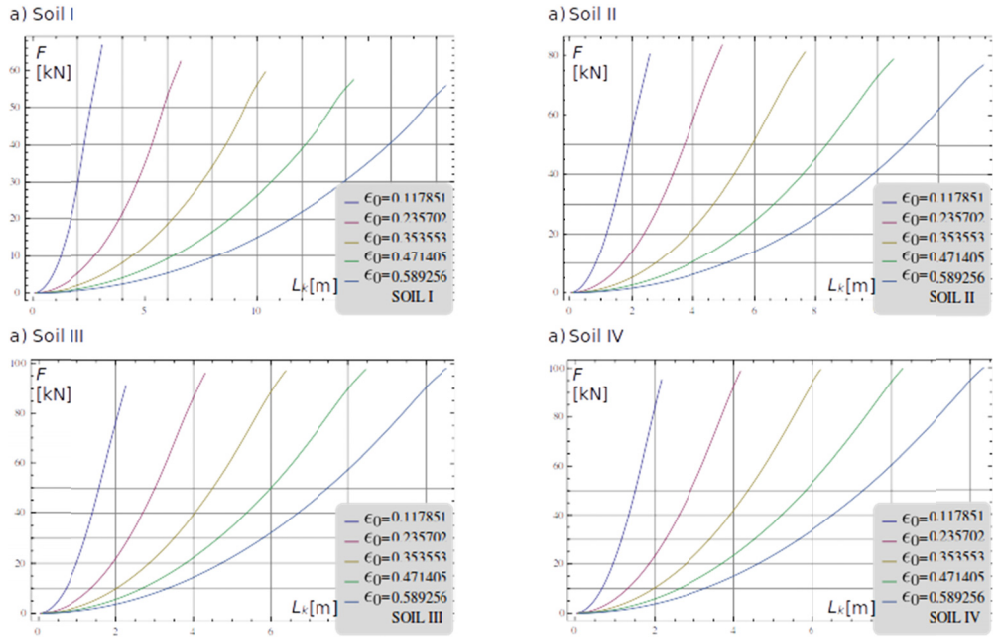


Fig. 13. Maximum force as a function of limited strip length $L_k$ and pile head displacement $\varepsilon_0$ for weak soil types as: (**a**) soil I, (**b**) soil II, (**c**) soil III, (**d**) soil IV

a mechanism that is estimated as the destructive force between the upper and lower bound approach with a number of simplifications for generalisation.

We observed that upon plastic deformation of the rough pile head, the mechanism may convert to a rotary form. This process has the desired effect for a maximum possible load. The estimation was presented, having an unexpected height from its initial value. The released ties in the joints were affected by a better use of the crack energy of the flysch, with greater displacements.

By assuming that the surfaces of cracks split the rock into two domains, it possible to analyse each independently. Another important element is confirming through experience that greater displacements of the material are caused by an increase in the horizontal load capacity of the layered rock.

Calculations were performed for the case of a horizontal arrangement of the layers to provide a good illustration of the analysed mechanical issues. In the future, the authors plan to conduct laboratory tests on soil samples, specifically for a wide range of vertical pressures using an oedometric modified apparatus for obtaining a more complete response of the material model. The results will be incorporated for complete flysch model based on random values of mechanical and geometric data.

## Acknowledgements

The authors are grateful to Wroclaw Networking and Supercomputing Centre for granting access to the computing infrastructure and the Mathematica program.

## References

Allasia P., Manconi A., Giordan D., Baldo M., Lollino G., 2013. *A New Approach for Near-Real-Time Monitoring of Surface Displacements in Landslide Hazard Scenarios*. Sensors **13**, 8285-8302.

Barton N.R., 1974. *A review of the shear strength of filled discontinuities in rock*. Norwegian Geotech. Inst. Publ. No. 105. Oslo: Norwegian Geotech. Inst.

Barton N.R., 1986. *Deformation phenomena in jointed rock*. Geotechnique **36** (2), 147-167.

Bednarczyk Z., 2014. *Landslide geohazard monitoring, early warning and stabilization control methods*. Studia Geotechnica et Mechanica **36** (1), 3-13.

Bertacchini E., Capitani A., Capra A., Castagnetti C., Corsini A., 2009. *Integrated surveying system for landslide monitoring, Valoria landslide (Apennines of Modena, Italy)*. Proceedings of FIG Working Week 2009. Eilat, Israel. ISBN 978-87-90907-73-0.

Bhat D.R., Yatabe R., Bhandari N.P. 2014. *Slow Shearing Rates' Effect on Residual Strength of Landslide Soils*. Geotechnical Special Publication **236**, 293-303.

Bhat D.R., Yatabe R., Bhandary N.P., 2013. *Study of preexisting shear surfaces of reactivated landslides from a strength recovery perspective*. Journal of Asian Earth Sciences **77**, 243-253.

Biernatowski K., Puła W., 1988. *Probabilistic analysis of the stability of massive bridge abutments using simulation methods*. Structural Safety **5** (11), 1-15.

Broniatowska M., Gaszyński J., 2006. *Strength tests of the Carpathian flysch rocks in the region of the constructed water reservoir Świnna Poręba*. ZSMG XXIX (english abstract).

Casagli N., Catani F., Del Ventisette C., Luzi G. 2010. *Monitoring, prediction, and early warning using ground-based radar interferometry*. Landslides **7**, 291-301.

Chowaniec J., Wójcik A., Mrozek T., Rączkowski W., Nescieruk P., Perski Z., Wojciechowski T., Marciniec P., Zimnal Z., Granoszewski W., 2012. *Osuwiska w województwie małopolskim. Atlas – przewodnik*. Departament Środowiska, Rolnictwa i Geodezji Urzędu Marszałkowskiego Województwa Małopolskiego, Zespół Geologii, pp. 143. (in Polish).

Collins B.D., Baum R.L., Mrozek T., Nescieruk P., Perski Z., Rączkowski W., Graniczny M., 2011. *Evaluation of Landslide Monitoring in the Polish Carpathians*. Open File Report.

Dzulynski S., Ksiazkiewicz M., Kuenen P., 1959. *Turbidites in flysch of the polish carpathian mountains*. Bulletin of the Geological Society of America **70** (8), 1089-1118.

Hillier S., 2006. Appendix A. *Mineralogical and chemical data*. in GM Reeves, I Sims, and JC Cripps eds., Clay materials used in construction: London, Geological Society, Engineering Geology Special Publications **21**, 449-459.

Hoek E., Brown E., 1980. *Underground excavations in rock*. The Institution of Mining and Metallurgy, London, UK

Jaeger J.C., Cook N.G., Zimmerman R.W., 2007. *Fundamentals of Rock Mechanics*. 4th ed. Oxford: Blackwell.

Kim B.H., Kaiser P.K., Grasselli G., 2007. *Influence of persistence on behaviour of fractured rock masses*. Geol. Soc. Lond. Special Publications **284**, 161-173.

Kiszka K., 2016. *Dendrochronological study of the Sawicki landslide activity in the Beskid Niski Mts (Polish Flysch Carpathians)*. Landform Analysis **32**, 9-26, doi: 10.12657/landfana.032.002.

Kozubal J., Puła W., Wyjadłowski M., Bauer J., 2013. *Influence of varying soil properties on evaluation of pile reliability under lateral loads*. Journal of Civil Engineering and Management **19** (2), 272-284.

Margielewski W., Pánek T., Táborík P., Urban J., Hradecký J., Szura C., 2010. *Gravitationally induced caves and other discontinuities detected by 2D electrical resistivity tomography: Case studies from the Polish Flysch Carpathians*. Geomorphology **123**, 165-180.

Muszyński Z., Rybak J., 2017. *Horizontal Displacement Control in Course of Lateral Loading of a Pile in a Slop*e. IOP Publishing Ltd IOP Conference Series: Materials Science and Engineering **245**, 1-8.

Puła W., 1997. *Reliability analysis of rigid piles subjected to lateral loads. Numerical models in geomechanics*. NUMOG VI. Proceedings of the Sixth International Symposium on Numerical Models in Geomechanics, Montreal, Eds S. Pietruszczak, G.N. Pande. Rotterdam, A.A.Balkema, 521-526.

Rączkowski W., 2004. *Landslide Hazard in the Carpathians during the recent 10 years*. Global Change **10**, 67-76.

Romeo S., Kieffer D.S., Matteo L., 2015. *Reliability of GBInSAR Monitoring in Ingelsberg Landslide Area (Bad Hofgastein, Austria*). Geotechnical Safety and Risk V,T. Schweckendiek et al. (Eds.). IOS Press. doi:10.3233/978-1-61499-580-7-803.

Shaw D.B., Weaver C.E., 1965. *The mineralogical composition of shales*. J. Sed. Pet. **35**, 213-222.